THE EUROPEAN
PHYSICAL JOURNAL A

Regular Article - Experimental Physics

Measurement of the $\gamma n \to K^0\Sigma^0$ differential cross section over the K^* threshold

BGOOD Collaboration

K. Kohl[1,a], T. C. Jude[1,b], S. Alef[1], R. Beck[2], A. Braghieri[3], P. L. Cole[4], D. Elsner[1], R. Di Salvo[6], A. Fantini[5,6], O. Freyermuth[1], F. Frommberger[1], F. Ghio[7,8], A. Gridnev[9], D. Hammann[1], J. Hannappel[1], N. Kozlenko[9], A. Lapik[10], P. Levi Sandri[11], V. Lisin[10], G. Mandaglio[12,13], R. Messi[5,6], D. Moricciani[11], V. Nedorezov[10], V. A. Nikonov[2,9], D. Novinskiy[9], P. Pedroni[3], A. Polonskiy[10], B.-E. Reitz[1], M. Romaniuk[5,14], G. Scheluchin[1], H. Schmieden[1], A. Stuglev[9], V. Sumachev[9], V. Tarakanov[9]

[1] Rheinische Friedrich-Willhelms-Universität Bonn, Physikalisches Institut, Nußallee 12, 53115 Bonn, Germany
[2] Rheinische Friedrich-Wilhelms-Universität Bonn, Helmholtz-Institut für Strahlen- und Kernphysik, Nußallee 14-16, 53115 Bonn, Germany
[3] INFN sezione di Pavia, Via Agostino Bassi, 6, 27100 Pavia, Italy
[4] Department of Physics, Lamar University, Beaumont, Texas 77710, USA
[5] INFN Roma "Tor Vergata", Via della Ricerca Scientifica 1, 00133 Rome, Italy
[6] Università di Roma "Tor Vergata", Dipartimento di Fisica, Via della Ricerca Scientifica 1, 00133 Rome, Italy
[7] INFN sezione di Roma La Sapienza, P.le Aldo Moro 2, 00185 Rome, Italy
[8] Istituto Superiore di Sanità, Viale Regina Elena 299, 00161 Rome, Italy
[9] Petersburg Nuclear Physics Institute NRC "Kurchatov Institute", Gatchina, Leningrad District 188300, Russia
[10] Russian Academy of Sciences Institute for Nuclear Research, Prospekt 60-letiya Oktyabrya 7a, 117312 Moscow, Russia
[11] INFN - Laboratori Nazionali di Frascati, Via E. Fermi 54, 00044 Frascati, Italy
[12] INFN sezione Catania, 95129 Catania, Italy
[13] Università degli Studi di Messina, Dipartimento MIFT, Via F. S. D'Alcontres 31, 98166 Messina, Italy
[14] Institute for Nuclear Research of NASU, 03028 Kyiv, Ukraine

V. Nedorezov and V. Sumachev are Deceased.

S. Alef, D. Hammann, B.-E. Reitz and G. Scheluchin are no longer employed in academia.

[a] e-mail: kohl@physik.uni-bonn.de (corresponding author)
[b] e-mail: jude@physik.uni-bonn.de

Abstract The differential cross section for the quasi-free photoproduction reaction $\gamma n \to K^0\Sigma^0$ was measured at BGOOD at ELSA from threshold to a centre-of-mass energy of 2400 MeV. Close to threshold the results are consistent with existing data and are in agreement with partial wave analysis solutions over the full measured energy range, with a large coupling to the $\Delta(1900)1/2^-$ evident. This is the first dataset covering the K^* threshold region, where there are model predictions of dynamically generated vector meson-baryon resonance contributions.

1 Introduction

Associated strangeness photoproduction is a crucial tool to study nucleon resonance spectra. A main motivation of the measurement of KY channels over the last 15 years has been to search for *missing resonances* which may only couple weakly to $N\pi$ final states [1,2]. $K^0\Sigma^0$ has a threshold at 1690 MeV, rendering the channel ideal to probe the third resonance region where many s-channel resonances up to high-spin states lie. Studying this reaction is therefore a requirement to constrain phenomenological models and partial wave analyses (PWA) which attempt to describe the nucleon excitation spectrum of known resonances. This includes PWA with dynamical coupled-channel frameworks [3–6], isobar models [7–14], and models incorporating Regge trajectories [15–17] to fix t-channel contributions. K^0 photoproduction data is also complementary to $K^\pm$ photoproduction as hadronic couplings can be related via isospin symmetry [18] and the absence of t-channel pseudo-scalar K exchange ensures s-channel resonance contributions are more dominant (however there are still K^* t-channel contributions).

Additionally, calculations based on vector meson-baryon interactions via coupled-channel unitary frameworks have predicted dynamically generated states contributing to $K^0\Sigma$ channels. A model by Ramos and Oset [19] explained a cusp-like structure observed in $K^0\Sigma^+$ photoproduction [20] at the K^* threshold from the destructive interference between amplitudes containing $K^*\Lambda$ and $K^*\Sigma$ intermediate states, and magnified by a proposed $N^*(2030)$ vector meson-baryon dynamically generated resonance at the $K^*\Sigma$ threshold. The model predicts that for photoproduction off the neutron, the interference of these amplitudes is constructive, resulting in a peak structure in the channel $\gamma n \to K^0\Sigma^0$.

The complexity of identifying the $K^0\Sigma^0$ final state has led to a lack of data compared to the $K^+\Lambda$ and $K^+\Sigma$ channels, where the only available dataset is from the A2 Collaboration and covers the first 150 MeV from threshold [21]. Motivation for the study of $K^0\Sigma^0$ photoproduction is therefore twofold. Firstly, to constrain phenomenological models and PWA used to describe the nucleon excitation spectrum. Secondly, to provide the first dataset over the K^* threshold region in an attempt to discriminate between models including "conventional" s-channel resonances and models predicting meson-baryon dynamically generated resonances beyond a qqq valence quark configuration. This paper reports a measurement of the differential cross section of the reaction $\gamma n \to K^0\Sigma^0$ from threshold to 2400 MeV, achieved with the BGOOD experiment [22] at the ELSA [23, 24] facility at Bonn University.

2 Experimental setup and running conditions

The presented data was taken using an ELSA electron beam of 2.9 GeV incident upon a thin radiator to produce a collimated beam of bremsstrahlung photons. The photon energies were determined by measuring the post bremsstrahlung electron momenta in the *Photon Tagger*. Two data taking periods with an 11 cm long target containing either liquid deuterium or hydrogen with identical beam conditions were used. The hardware trigger, which was the same for both data taking periods, required a signal in the Photon Tagger and an energy deposition of at least 200 MeV in the BGO Rugby Ball. Details on the characterization and modelling of the trigger are in Ref. [25]. The signal was extracted from the deuterium data and the hydrogen data was used to subtract background originating off the the proton in the deuterium. The integrated photon flux from threshold to a centre-of-mass energy[1] of 2400 MeV was $6.39 \cdot 10^{12}$ and $5.78 \cdot 10^{12}$, respectively.

The BGOOD experiment is composed of a magnetic forward spectrometer complemented with a central BGO calorimeter [22]. The *BGO Rugby Ball*, is composed of 480 BGO crystals, which surround the target and cover a polar angle range of $25° < \theta_{lab} < 155°$. Each crystal spans $6°$ to $10°$ in the polar angle θ_{lab}, $11.25°$ in the azimuthal angle ϕ and has a depth of 24 cm, corresponding to 21 radiation lengths. The time resolution of 2 ns allows for a clean separation of multiple photons for neutral meson reconstruction. A minimal required energy deposition of 1.5 MeV per individual crystal and 25 MeV per crystal cluster suppresses neutron background. A barrel type arrangement of plastic scintillators interior to the BGO Rugby Ball is utilized to veto charged particles. The forward spectrometer covers the angular range $1° < \theta_{lab} < 12°$. A series of tracking detectors sandwiching the open dipole magnet [22] are used for charged particle identification and momentum reconstruction. The small intermediate range is covered by a segmented array of 96 plastic scintillators for charged particle detection.

3 Selection of $\gamma n \to K^0\Sigma^0$ events

K^0 candidates were identified via the decay $K_S^0 \to \pi^0\pi^0 \to (\gamma\gamma)(\gamma\gamma)$ in the BGO Rugby Ball. Two photon pairs were required where the invariant masses were within 30 MeV/c^2 of the π^0 mass, which corresponds to $\pm 2\sigma$.

Three additional selection criteria were used to isolate the reaction channel. First, the missing mass to the K^0 candidates was required to be consistent with the Σ^0 mass, lying between 1150 and 1250 MeV/c^2. Secondly, identification of the photon from the decay $\Sigma^0 \to \gamma\Lambda$ was required. To achieve this, photons which were not identified as a π^0 decay photon were boosted into the rest frame of the Σ^0. Figure 1 shows the energy of the boosted γ in this frame, where a peak at 75 MeV from the two-body Σ^0 decay is expected. A small peak is visible over a large background at this energy, which is consistent with the simulated data. The decay photon from the channel $\gamma p \to K^+\Sigma^0$ is also shown, where the signal is cleaner[2]. Events were selected where the photon energy was between 54 MeV and 96 MeV, corresponding to $\pm 3\sigma$.

The final selection criterion required the detection of exactly two charged particles consistent with the decay $\Lambda \to \pi^- p$. The Λ momentum was calculated from the missing momentum to the K^0 and the photon from the Σ^0 decay, and the angle between the charged particles and the Λ was determined. This angle must lie within the kinematically allowed region shown in Fig. 2. Nearly all π^- and p were detected in the BGO Rugby Ball or SciRi, where no completely clean identification between them could be made. All events where at least one charged particle was within the angular limit for

---

[1] To correctly determine the centre-of-mass energy the Fermi-momentum of the target particle needs to be known, however since this was not possible event by event, the target was assumed to be at rest.

[2] This technique was used to identify the $K^+\Sigma^0$ channel in Ref. [26].
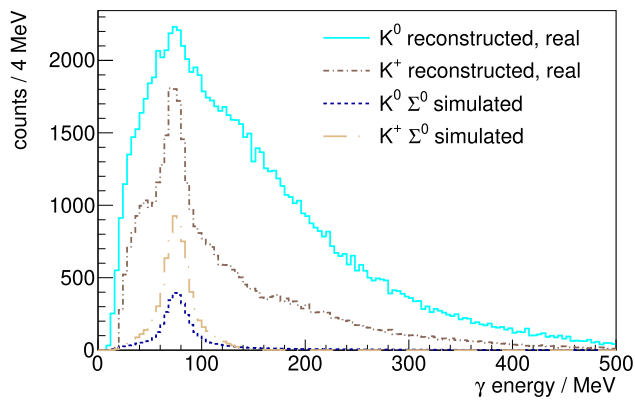
Fig. 1 Photon energy spectrum in the Σ^0 rest frame for real and simulated data for the channels $\gamma p \rightarrow K^+ \Sigma^0$ and $\gamma n \rightarrow K^0 \Sigma^0$ at an arbitrary scale
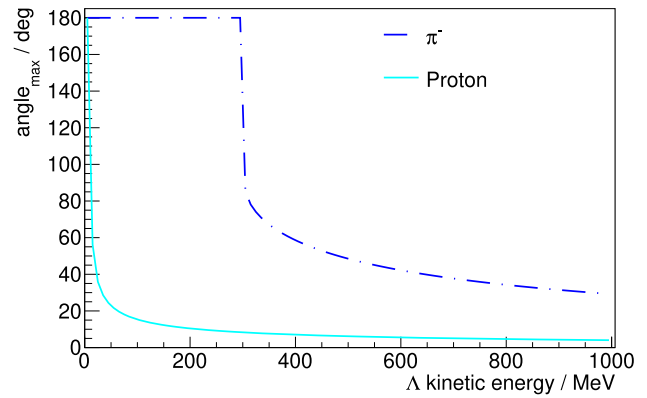
the proton and the other for the π^- were therefore retained. The small angle allowed between the Λ and proton in particular, provided a vital constraint for removing other misidentified reaction channels. An additional $10°$ was permitted to account for detector resolution and the unmeasured Fermi-momentum of the target nucleon within the deuteron.

For a given event, all combinations of particle assignment to the five neutral and two charged particles were retained if they passed the selection criteria. No kinematic fit was applied as the lack of energy information of the detected charged particles combined with the unknown target Fermi-momentum prevented a full four-momentum constraint. Figure 3 shows how the different selection cuts affect the invariant mass distribution of the two π^0 system. Figure 3a depicts simulated $\gamma n \rightarrow K^0 \Sigma^0$ data, where increasing the selection criteria removes the low mass shoulder originating from combinatorial background, for example misidentifying a γ from the Σ^0 decay as a π^0 decay γ. This background is small after including all selection criteria and was estimated as contributing a systematic uncertainty of 3 %. Figure 3b depicts real data using a deuterium target, where the peak corresponding to the K^0 invariant mass becomes increasingly pronounced from the background distribution with increased selection criteria.

Background from reaction channels off the proton in the deuteron was subtracted by applying the same selection criteria to the liquid hydrogen target dataset. The hydrogen data was scaled according to the ratio of the photon beam flux and target densities. To account for the broadening of momentum and mass distributions caused by the unmeasured Fermi motion, the proton target four-momentum in the computation of kinematic quantities was smeared according to the momentum distribution of nucleons in deuterium [27]. Figure 4 shows the scaled hydrogen data together with the deuterium data and the resulting spectrum after subtracting hydrogen data from deuterium data.
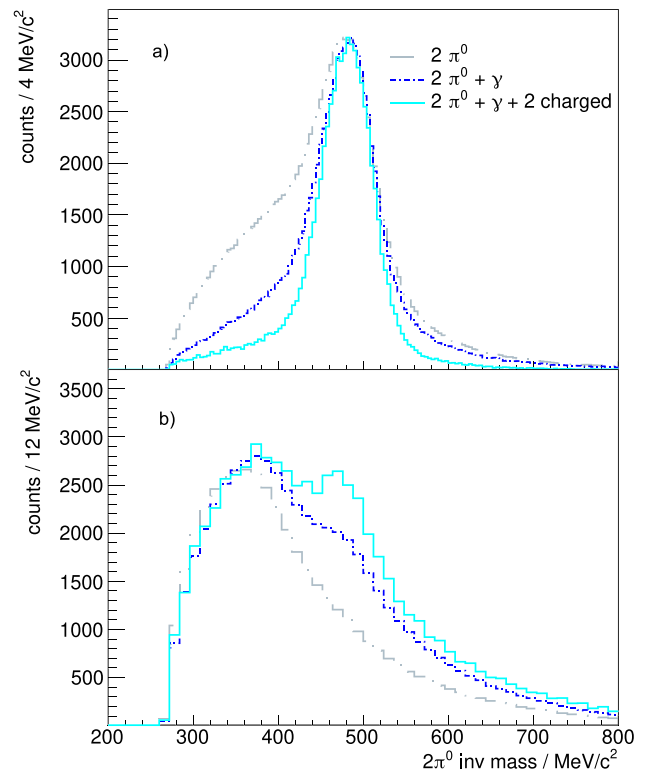

Fig. 2 Maximum possible angle between either the proton or the π^- and Λ as a function of Λ kinetic energy in the decay $\Lambda \rightarrow p\pi^-$

Fig. 3 The invariant mass distribution of the $2\pi^0$ system for all measured W and $\cos(\theta)$ intervals after different selection criteria for **a** simulated $\gamma n \rightarrow K^0 \Sigma^0$ and **b** real data using a deuterium target. The selection criteria are: only two π^0, two π^0 and γ from Σ^0 decay, two π^0, γ and two charged particles from Λ decay. The grey and dark blue distributions are scaled to approximately match the maximum height

Two methods were used to fit to the $K^0 \Sigma^0$ signal and remaining background. The first used simulated phase-space distributions of the dominant background channels, referred to later as *PS*. Simulated data was used to determine the fraction of background channel events passing the selection criteria. The dominant channels were found to be multi-pion production ($\gamma n \rightarrow 3\pi N$ and $\gamma n \rightarrow 4\pi N$) and $\gamma n \rightarrow \eta n$, all of which gave almost identical $2\pi^0$ invariant mass spec-
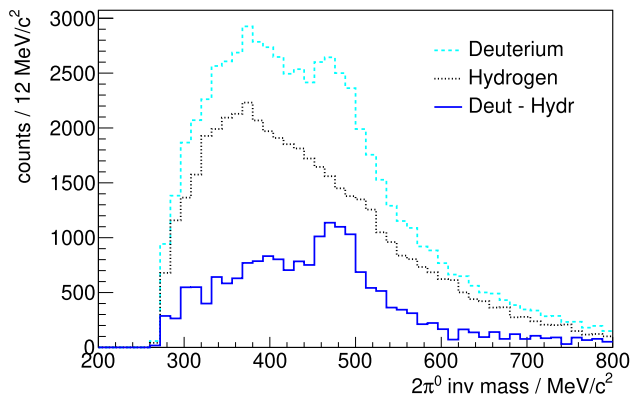
Fig. 4 The invariant mass distribution of the $2\pi^0$ system after all selection criteria for deuterium and hydrogen data. The hydrogen data is scaled by luminosity and subtracted from the deuterium data

tra. The required topology of five neutral and two charged particles was satisfied by these background channels either exactly, or by missing a particle in small acceptance gaps in the experimental setup, or by falsely identifying an additional particle due to split-off clusters in the BGO Rugby Ball and particles scattering off detector components. The channel $\gamma n \to 3\pi^0 n$ was chosen as representative of the multi-pion channels and used to describe the background distribution. Other channels were found to provide negligible contributions.

The second method, later referred to as *RD*, used real data to describe the background. To generate this distribution, a K^0 candidate and an additional photon were required, however this photon was not identified as a Σ^0 decay photon candidate and there was no selection criteria on charged particle multiplicity or topology.

In both cases, the signal shape was phase-space generated using simulated $K^0\Sigma^0$ data and a full Geant4 [28] simulation of the experimental setup. Roofit [29] was used to fit the data with a maximum likelihood fit. Figure 5 shows fit examples using the PS background description in the angular range $0.2 < \cos\theta_{CM}^K < 0.5$, where $\cos\theta_{CM}^K$ is the cosine of the centre-of-mass polar angle of the K^0.

The limited statistical precision reduces the usefulness of χ^2 distributions. Instead a hypothesis test was performed to prove the necessity of the simulated signal distribution to describe the data. The test gives the probability of the data following a given distribution which is only comprised of background, the hypothesis of which is denoted H_0. This is achieved by creating 10,000 Monte Carlo (MC) samples from the background distributions each with the same statistical precision as the real data distributions. Each MC sample is fitted twice. The first fit is with background (BG) only, the second is with background and signal (BG+S). ζ^2, given in Eq. 1 is calculated for each fit, where N_{fit} and N_{data} are the number of events in each bin of the fitted spectrum for the
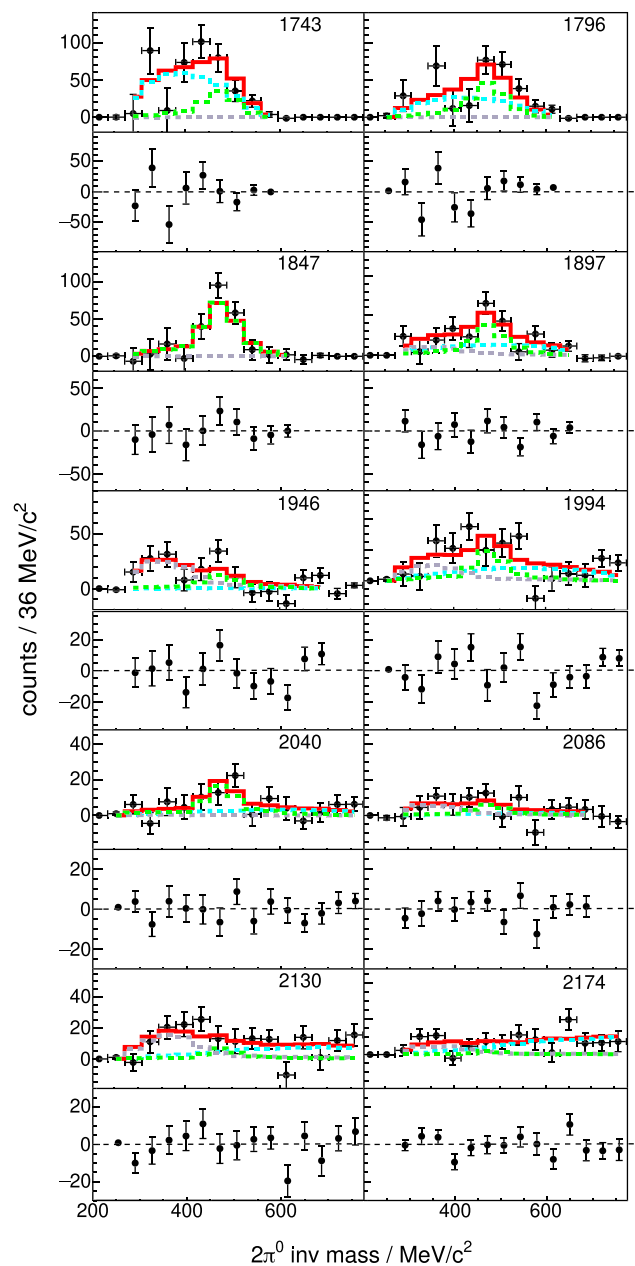

Fig. 5 Example of fits to the $2\pi^0$ invariant mass spectrum. The angular region is show from $0.2 < \cos\theta_{CM}^K < 0.5$ in 10 energy bins. The centre of each energy bin is given as W in MeV in the top right corner. Black points are measured data, the signal is shown in green. The two background channels $\gamma n \to 3\pi^0 n$ and $\gamma n \to \eta n$ are shown in light blue and gray. The sum of all channels is depicted as a solid red line. The residuals are plotted under each fit

fitted function and the data respectively, and ΔN_{data} is the corresponding error.

$$\zeta^2 = \sum_{bins} \left(\frac{N_{fit} - N_{data}}{\Delta N_{data}} \right)^2 \quad (1)$$

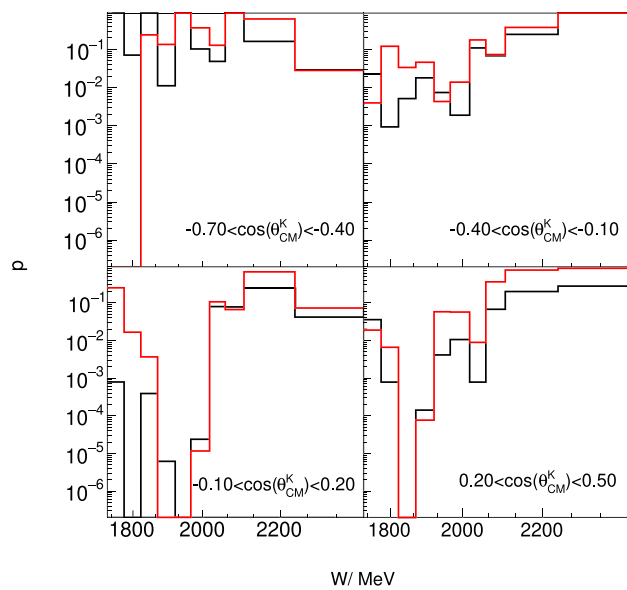**Fig. 6** p as a function of W for the two different background distributions. The black line corresponds to a background distribution using PS description, the red line corresponds to a background distribution using RD description respectively

For each MC sample the difference is calculated:

$$\Delta\zeta^2 = \zeta^2(BG) - \zeta^2(BG+S) \qquad (2)$$

This is repeated for the real data, denoted $\Delta\zeta^2_{\text{real}}$. The distribution of $\Delta\zeta^2$ for the 10,000 MC samples under the hypothesis H_0 is denoted $g(\Delta\zeta^2|H_0)$.

A measure of agreement with H_0 can then be calculated from Eq.3:

$$p = \int_{\Delta\zeta^2_{\text{real}}}^{\infty} g(\Delta\zeta^2|H_0) \qquad (3)$$

Figure 6 shows p using the two background descriptions PS and RD. Both descriptions generally agree with each other. p is low where the signal gives a significant contribution to the fitted spectrum, indicating that a background distributions alone is not sufficient to describe the data.

An alternative method to separate signal and background was made using side band subtraction techniques [30]. The resulting yields were in agreement to the fitting methods described above.

Fitting to the K^0 invariant mass does not discriminate between $\gamma n \rightarrow K^0\Sigma^0$ and $\gamma n \rightarrow K^0\Lambda$, however, the selection criteria strongly suppressed the contribution from $\gamma n \rightarrow K^0\Lambda$. Simulated data and cross section measurements from Ref. [31] were subsequently used to determine and subtract the remaining contribution of $K^0\Lambda$ to the $K^0\Sigma^0$ yield. This was a small contribution and largest near threshold, with for example 16 % and 2 % of the extracted yield in
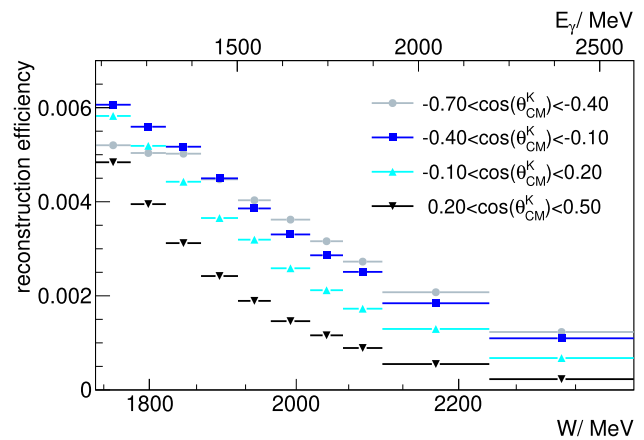

Fig. 7 Reconstruction efficiency as a function of energy for four different $\cos\theta^K_{\text{CM}}$ intervals

Table 1 Sources and values of systematic uncertainties (not including the fitting systematic uncertainty)

Source	% Error
Photon flux	4
Target length	1
Beam energy calibration	1
Modelling of hardware triggers	1
π^0 identification	3
$\Sigma^0 \rightarrow \gamma\Lambda$ identification	6
Selection of the missing (Σ^0) mass	3
Charged particle identification	4
Combinatorial background	3
Subtraction of hydrogen background	5
$K^0\Lambda$ subtraction	1
Summed in quadrature	11

the angular bin $0.2 < \cos\theta^K_{\text{CM}} < 0.5$ at center-of-mass energies 1796 MeV and 2040 MeV respectively.

The reconstruction efficiency is depicted in Fig. 7 as a function of energy for four different $\cos\theta^K_{\text{CM}}$ ranges. This includes the branching ratios of the K^0 eigenstates K^0_S and K^0_L and the detected K^0_S and Λ decay modes, which limits the efficiency to $\approx 10\%$. Requesting five neutral particles in the central calorimeter further reduces the efficiency to below 1 %. No structures are seen that could cause artefacts in the measured cross section.

Table 1 shows the systematic uncertainties. The identification of the photon from the decay $\Sigma^0 \rightarrow \gamma\Lambda$ and the subtraction of hydrogen background are the dominating uncertainties at 6% and 5% of the measured cross section, respectively. The uncertainty on the photon flux normalization was determined as explained in Ref. [25]. Systematic uncertainties specific to this analysis were estimated by varying the selection criteria at each step and determining the effect on
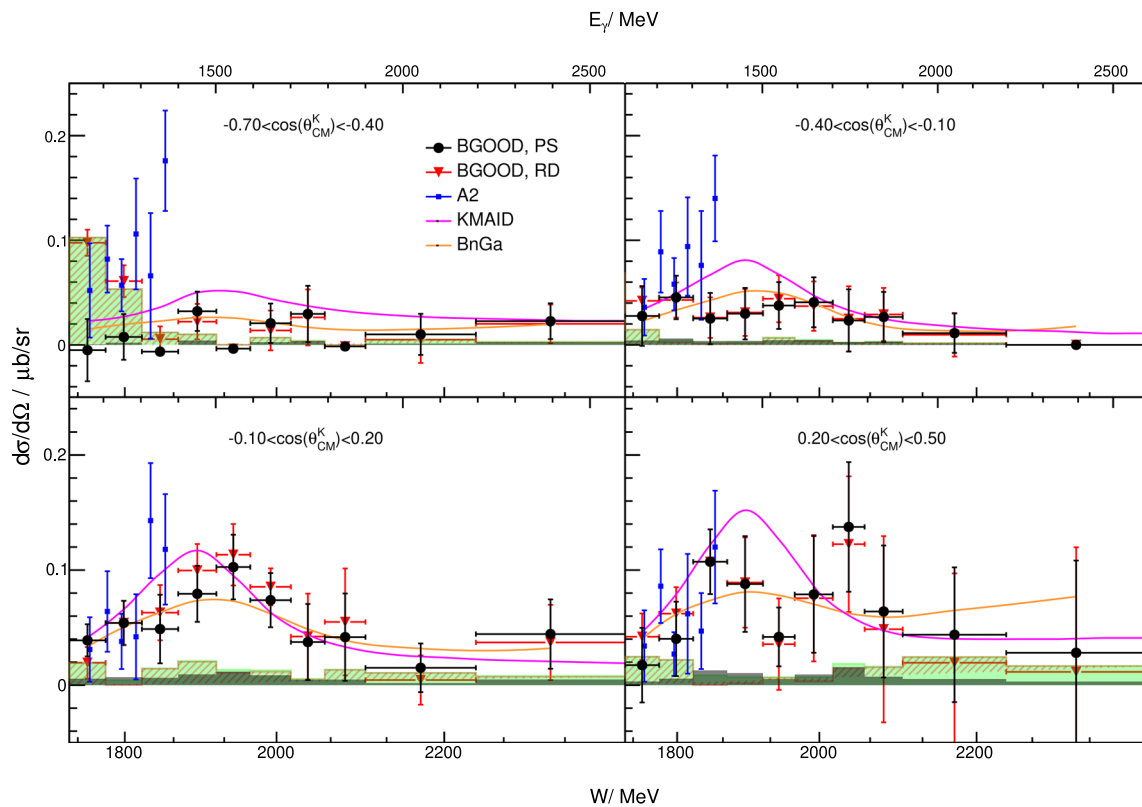
Fig. 8 $\gamma n \to K^0 \Sigma^0$ differential cross section as a function of W in four bins in $\cos \theta_{CM}^K$ for both fitting methods RD and PS (red triangles and black circles respectively). Vertical error bars are the statistical error, horizontal error bars indicate the bin width. Systematic errors are split into *scaling errors* shown as grey columns and *fitting errors* shown as dashed red columns. The sum in quadrature of both is shown as green columns. Data from Akondi et al. (A2 Collaboration)[21] is shown in blue squares, with median values of $\cos \theta_{CM}^K$ of -0.625, -0.375, 0.125 and 0.375. Calculations from Kaon MAID[11] and BnGa[32] are shown as magenta and orange lines respectively

the extracted cross section. The systematic uncertainty of fitting is determined as the difference between the cross section of the two methods to fit the background (RD and PS). While all other systematic uncertainties are a constant fraction of the measured cross section and therefore can only change the global scaling of the dataset, the fitting uncertainties permit point to point fluctuations of the data points. These uncertainties are therefore shown separately in Fig. 8.

4 Results

The differential cross section for $\gamma n \to K^0 \Sigma^0$ is shown in Fig. 8 as a function of energy in four bins in $\cos \theta_{CM}^K$. The two methods used to describe and subtract background show a good agreement, with the exception of the most backward angle bin, $-0.7 < \cos \theta_{CM}^K < -0.4$, where there is a discrepancy of up to $0.1 \, \mu$b/sr in the first two energy bins from threshold to $W = 1823$ MeV. This is due to limited phase space in the $2\pi^0$ invariant mass spectrum preventing a clean separation of signal and background. The data of Akondi

et al. (A2 Collaboration)[21] are shown as the blue squares from threshold to $W = 1855$ MeV. When combining the statistical and systematic uncertainties of both datasets (the systematic uncertainty of the A2 data varies from 0.001 to $0.004 \, \mu$b/sr), there is reasonable consistency over most of the kinematic coverage, however the A2 data generally appears higher. This is most pronounced at the two most backward angles at $W = 1855$ MeV, where there is a discrepancy of approximately $1\sigma - 2\sigma$ beyond the combined uncertainties.

Calculations from the Kaon MAID effective Lagrangian model[11] and the Bonn-Gatchina Partial Wave analysis (BnGa)[32] are shown as the magenta and orange lines respectively. The BnGa calculation includes dominant contributions from S_{11} and P_{11} partial waves and gives an agreement to the data over the full measured $\cos \theta_{CM}^K$ range. The Kaon MAID calculation also appears to have a reasonable agreement in the two most forward $\cos \theta_{CM}^K$ intervals, whereas in the two backward intervals the calculation lies approximately between this data and the A2 data. The Kaon MAID model includes resonant contributions from $\Delta(1650)1/2^-$, $N(1710)1/2^+$,

$N(1720)3/2^+$, $\Delta(1900)1/2^-$ and $\Delta(1910)1/2^+$. The peak at $W = 1900$ MeV observed in the data most prominently in the interval $-0.10 < \cos\theta_{CM}^K < 0.20$ is described by the large coupling to the $\Delta(1900)1/2^-$.

The model by Ramos and Oset [19] predicted a peak at the K^* threshold caused by a vector-meson baryon dynamically generated state. This dataset does not exclude a structure at $W \approx 2040$ MeV and $0.20 < \cos\theta_{CM}^K < 0.50$, however the current statistical precision does not permit a conclusion and further data is required to discriminate between phenomenological models in this energy range.

Contributions from final state interactions can not be disregarded without additional studies, however calculations for quasi-free photoproduction off the deuteron of K^+Y [33,34] show them to be negligible over the kinematic range presented here.

5 Conclusions

A first measurement of the reaction $\gamma n \rightarrow K^0\Sigma^0$ is presented from threshold to 2400 MeV, spanning the region of the K^* threshold. The channel was identified via the decays $K_S^0 \rightarrow \pi^0\pi^0$ and $\Sigma^0 \rightarrow \Lambda\gamma \rightarrow (p\pi^-)\gamma$ at the BGOOD experiment. Two different methods were used to describe background from other reaction channels passing the selection criteria, which after fitting to $2\pi^0$ invariant mass spectra to extract the signal proved compatible. The data are consistent with existing data and well described by PWA solutions. Improved statistical precision and an extension to more forward $\cos\theta_{CM}^K$ is required to fully characterize and discriminate between model calculations.

In BnGa no resonances are put in a priori. Instead poles emerge from the K Matrix formalism within specific partial waves. What is included here is S11 and P11 partial waves.

Data Availability Statement This manuscript has no associated data or the data will not be deposited. [Authors' comment: The data is available upon request.].

References

1. S. Capstick, W. Roberts, Prog. Part. Nucl. Phys. **45**, S241 (2000)
2. U. Loring, B.C. Metsch, H.R. Petry, Eur. Phys. J. A **10**, 395 (2001)
3. A.V. Anisovich et al., Eur. Phys. J. A **34**, 243 (2007)
4. A.V. Anisovich et al., Eur. Phys. J. A **50**, 129 (2014)
5. J. Müller et al., Phys. Lett. B **803**, 135323 (2020)
6. D. Rönchen, M. Döring, U.G. Meißner, Eur. Phys. J. A **54**, 110 (2018)
7. D. Skoupil, P. Bydžovský, Phys. Rev. C **93**, 025204 (2016)
8. D. Skoupil, P. Bydžovský, Phys. Rev. C **97**, 025202 (2018)
9. T. Mart, C. Bennhold, Phys. Rev. C **61**, 012201 (2000)
10. S. Clymton, T. Mart, Phys. Rev. D **96**, 054004 (2017)
11. F.X. Lee, T. Mart, C. Bennhold, L.E. Wright, Nucl. Phys. A **695**, 237 (2001)
12. S. Janssen, J. Ryckebusch, D. Debruyne, T. Van Cauteren, Phys. Rev. C **65**, 015201 (2002)
13. S. Janssen, J. Ryckebusch, W. Van Nespen, D. Debruyne, T. Van Cauteren, Eur. Phys. J. A **11**, 105 (2001)
14. S. Janssen, D.G. Ireland, J. Ryckebusch, Phys. Lett. B **562**, 51 (2003)
15. L. De Cruz, T. Vrancx, P. Vancraeyveld, J. Ryckebusch, Phys. Rev. Lett. **108**, 182002 (2012)
16. L. De Cruz, J. Ryckebusch, T. Vrancx, P. Vancraeyveld, Phys. Rev. C **86**, 015212 (2012)
17. P. Bydžovský, D. Skoupil, Phys. Rev. C **100**, 035202 (2019)
18. T. Mart, Phys. Rev. C **83**, 048203 (2011)
19. A. Ramos, E. Oset, Phys. Lett. B **727**, 287 (2013)
20. R. Ewald et al., Phys. Lett. B **713**, 180 (2012)
21. C. Akondi et al., Eur. Phys. J. A **55**, 202 (2019)
22. S. Alef et al., Eur. Phys. J. A **56**, 104 (2020)
23. W. Hillert, Eur. Phys. J. A **28S1**, 139 (2006)
24. W. Hillert et al., EPJ Web Conf. **134**, 05002 (2017)
25. S. Alef et al., Eur. Phys. J. A **57**, 80 (2021)
26. T.C. Jude et al., Phys. Lett. B **820**, 136559 (2021)
27. M. Lacombe et al., Phys. Rev. C **21**, 861 (1980)
28. J. Allison et al., Nucl. Instrum. Meth. A **835**, 186 (2016)
29. W. Verkerke, eConf **C0303241**, MOLT007 (2003)
30. K. Kohl, Ph.D. thesis, Rheinische Friedrich-Wilhelms-Universität Bonn (2022)
31. N. Compton et al., Phys. Rev. C **96**, 065201 (2017)
32. A. Sarantsev, private communication (2022)
33. K. Miyagawa, T. Mart, C. Bennhold, W. Glockle, Phys. Rev. C **74**, 034002 (2006)
34. A. Salam, H. Arenhovel, Phys. Rev. C **70**, 044008 (2004)